Rheologica Acta
https://doi.org/10.1007/s00397-025-01503-0

ORIGINAL CONTRIBUTION

Flow of microgels with different softness at the interface reproduced by a multi-Hertzian model

Tom Höfken[1] · José Ruiz-Franco[2,3] · Andrea Scotti[4] · Emanuela Zaccarelli[5,6]

Received: 24 January 2025 / Revised: 12 May 2025 / Accepted: 29 May 2025

Abstract

Once surface active colloids, such as microgels, adsorb to an interface, they modify the viscoelastic properties of the interface. In contrast to what happens in bulk, the elastic properties have a non-monotonic dependence on the generalized area fraction. In this study, we describe this phenomena by performing molecular dynamic simulations of effective pair potentials in two dimensions. Our potential model is constructed by taking available interfacial rheology experimental results as a starting point. From this knowledge, we need to take into account, for very dense monolayers, that the interaction between adsorbed microgels has to consider multiple factors, including an increase in microgel stiffness when compressed and the presence of a dense inner core region. To account for these properties, we adopt a square-shoulder multi-Hertzian model, which predicts equilibrium structures and rheological properties in qualitatively agreement with experiments. Crucially, this model avoids the reentrant liquid behavior commonly observed with soft Hertzian-based pair potentials at high concentrations. Building on these insights, we thus explore the parameter space of this potential, providing novel predictions for dense monolayers composed of differently crosslinked microgels, awaiting for experimental investigation in the near future.

Keywords Microgels · Multi-Hertzian · Rheology

Introduction

Microgels, crosslinked polymer networks swollen by a good solvent combine properties of classical colloidal particles and polymers (Plamper and Richtering 2017; Lyon and Fernandez-Nieves 2012). Their inherent softness enables them to isotropically deswell, interpenetrate, or deform in response to changes in the external osmotic pressure or due to the interaction with their neighbor (Scotti et al. 2022, 2018; Del Monte and Zaccarelli 2024). Suspensions of microgels serve as an excellent model system for studying the dependence on softness of the glass transition and the flow behavior of soft colloids, both in bulk and at interfaces (Purnomo et al. 2008; Stieger et al. 2004; Huang et al. 2017; Scotti et al. 2020; Bassu et al. 2024). Understanding how the compressibility of individual particles translate into macroscopic behavior is a key step in designing new materials (Lyon et al. 2009). Over the years, a wide variety of microgel architectures have been experimentally realized (Karg et al. 2019). The crosslinking fraction c is one of the simplest parameters to adjust during synthesis, directly influencing the swelling ratio (Sbeih et al. 2019; Lopez and Richtering 2017) and the single particle bulk modulus (Houston et al. 2022; Höfken et al. 2024) of the microgel. Moreover, complex architectures such as hollow (Nayak et al. 2005), core-shell (Karg et al. 2008), anisotropic (Crassous et al. 2015) and ultra-low crosslinked (ULC) microgels (Bachman et al. 2015) have been put forward.

✉ Andrea Scotti
andrea.scotti@fkem1.lu.se

✉ Emanuela Zaccarelli
emanuela.zaccarelli@cnr.it

1 Institute of Physical Chemistry, RWTH Aachen University, Landoltweg 2, 52074 Aachen, Germany

2 Department of Condensed Matter Physics, University of Barcelona, Carrer de Martí i Franquès 1, 08028 Barcelona, Spain

3 Institute of Complex Systems (UBICS), University of Barcelona, Carrer de Martí i Franquès 1, 08028 Barcelona, Spain

4 Division of Physical Chemistry, Lund University, Lund SE-22100, Sweden

5 Italian National Research Council - Institute for Complex Systems (CNR-ISC), Sapienza University of Rome, Piazzale Aldo Moro 5, 00185 Rome, Italy

6 Department of Physics, Sapienza University of Rome, Piazzale Aldo Moro 2, 00185 Rome, Italy

Published online: 11 June 2025

When confined at a liquid-liquid interface, such as air-water or oil-water, the deformability of microgels makes them able to undergo significant structural changes to minimize interfacial tension (Rey et al. 2020; Bochenek et al. 2022). While low-crosslinked microgels spread more extensively, highlighting their polymeric character, the more crosslinked ones adopts a so-called "fried egg" characteristic shape (Scotti et al. 2019). This is due to the fact that microgels are not homogeneous networks, but they contain a density gradient within their polymer distribution, due to the higher reactivity of crosslinkers with respect to monomers (Stieger et al. 2004). This gives rise to a denser core in the center of the microgel, comparable to the yolk of the egg, surrounded by a fuzzy corona, which undergoes a large stretching at the interface and resemble the white of the egg (Camerin et al. 2019).

Once the structure of a single microgel with the interface is understood, it becomes possible to study the properties of concentrated monolayers, where interparticle interactions dictate the structural and elastic properties of the interface. Experimentally they can be probed by *in-situ* interfacial rheology combined with *ex-situ* atomic force microscopy (AFM). Recently, we carried out such an experimental investigation for two explicit cases of such monolayers: one composed of regularly crosslinked microgels with $c = 5$ mol% (Schmidt et al. 2023) and another of ULC microgels (Ruiz-Franco et al. 2024). The latter are synthesized in the absence of crosslinkers, with self-binding of monomers randomly happening within the network and yielding an effective crosslinker concentration $\lesssim 0.3$ mol% (Hazra et al. 2023). The experiments have been complemented by molecular dynamics simulations, which give insight on the central role of the different particle compressibility in determining the flow properties of the monolayer.

In particular, it was found that the elasticity of the monolayer, quantified by the yield-stress or by the storage modulus, shows a non-monotonic behavior with increasing generalized area fraction (ζ_{2D}). Starting from dilute conditions, the interface stiffens with increasing concentration until the glass transition is reached. After reaching a maximum the yield stress as well as the storage modulus decrease at higher compression, before rising again at very high ζ_{2D} This behavior, shared by both studied types of microgels, leads to the existence of so-called 'isoelastic' points, where the monolayer stores the same amount of energy at vastly different concentrations and compression levels. Both static and dynamic properties of the monolayer were qualitatively reproduced by simulations, based on simple pair-potential models. In truth, the non-monotonic course of dynamical quantities has long been predicted by soft pair-potentials, for example the diffusion coefficient of a classical Hertzian model (Pàmies et al. 2009; Berthier et al. 2010). However, these models usually overestimate the acceleration of the dynamics, predicting a re-entrant liquid phase (Berthier et al. 2010), that is not observed either experimentally in soft colloids such as microgels (Conley et al. 2017; Philippe et al. 2018) or by simulations of monomer-resolved models (Del Monte and Zaccarelli 2024).

For dense microgel monolayers probed by interfacial rheology, the system also remains solid beyond the glass transition, different from Hertzian predictions (Schmidt et al. 2023). Consequently, we proposed to modify the potential to include additional terms, yielding a so-called multi-Hertzian model (Bergman et al. 2018) for ULC microgels (Ruiz-Franco et al. 2024). However, we still need to validate the multi-Hertzian model for experimental measurements of regularly crosslinked microgels, too. This is the first aim of the present work.

Hence, in the following, we will work with a multi-Hertzian pair potential that is built from three key components: (i) a regular Hertzian to describe the interaction at low deformation, (ii) a square-shoulder core term to model the dense microgel core and (iii) additional Hertzian terms that model the stiffening of the entire monolayer at high compression. The first two contributions directly relate to structural microgel properties and can be linked to their crosslinking fraction. For instance, a higher amount of crosslinker density results in an overall stiffer particle, which increases the Hertzian strength at low deformation (Rovigatti et al. 2019). The second term arises from the fact that crosslinked microgels are not homogeneous, so that their denser cores remain stiffer than the corona in the adsorbed state (Bochenek et al. 2022; Schulte et al. 2022). It was observed that at high enough compression, the microgels develop an incompressible limit for $c = 5$ mol%, while such a feature is absent for ULC microgels. Finally, the third and inner term is an indirect consequence of the monolayer compression, a many-body effect, within our simple pair interaction description. Indeed, upon decreasing the generalized area fraction of the monolayer, each individual microgel is compressed, interpenetrating with neighboring particles, so that the layer thickness increases (Gerelli et al. 2024). This gives rise to an additional elastic contribution in our model, which sets in at high enough compression. For ULC microgels, the strength of this term was empirically tuned to prevent re-entrant liquid behavior, which is not observed experimentally. The same approach is performed here for $c = 5$ mol% microgels.

Once we have validated the model against the experimental results reported in the literature (Schmidt et al. 2023; Ruiz-Franco et al. 2024), we then leverage computer simulations to scan the parameter space of this new pair potential and make qualitative statements about the relation between particle properties and their rheological behavior as a function of generalized area fraction. To this aim, we conduct equilibrium molecular dynamics to study the structuring in the monolayer at rest and non-equilibrium simulations under an

external steady shear and oscillatory shear, the latter to compute storage and loss moduli. We then generalize the results to additional values of the crosslinking fraction, not yet studied experimentally, in order to provide a general framework for predicting monolayer elastic properties at the interface that can be used as a reference in future experimental studies.

The manuscript is thus organized as follows. We start by introducing the simulation models and methods in Section "Models and methods". We then report the results in Section "Results", which are organized in three main subsections. First, we validate the multi-Hertzian model against $c = 5$ mol% interfacial rheology experiments carried out in Ref. (Schmidt et al. 2023) in Subsection "Validation for 5 mol% crosslinked microgels". Then, we vary the parameters of the multi-Hertzian model to assess their individual influence of the rheological behavior of the monolayer in Subsection "Exploring the parameter space". Next, we calculate rheological properties of a set of parameters that should represent $c = 1$ mol% and $c = 10$ mol% microgels, reporting the properties of the monolayer as a function not only of ζ_{2D} but also of crosslinker concentration in Subsection "Variation of crosslinking". Finally, we draw our conclusions and perspectives in Section "Conclusion".

Models and methods

The interaction between two individual microgels that are spread at the liquid-liquid interface has been shown to be well described by using a Hertzian model in two dimensions (Camerin et al. 2020):

$$V_H(r) = \frac{\pi Y d^2 (1 - r/d)^2}{2 \ln\left(\frac{2}{1-r/d}\right)}, \tag{1}$$

where Y denotes the 2D Young modulus, while d is the diameter of the discs, and fixes the unit length of our simulations. However by increasing the generalized area fraction, microgels start to be confined in a dense monolayer, which increases in density and thickness and the pure Hertzian is no longer accurate in describing the experimental results (Schmidt et al. 2023). To account for the more repulsive interactions at higher deformation, we adopt a multi-Hertzian approach, expressed as:

$$V_{MH}(r) = V_H(r, d, Y) + V_H\left(r, \frac{d + d_{dens}}{2}, \sqrt{Y \cdot Y_{dens}}\right) + V_H(r, d_{dens}, Y_{dens}). \tag{2}$$

Effectively, an additional small Hertzian disc with diameter $d_{dens} = 0.9d$ and Young modulus Y_{dens} interacts with the other particles and their centers. Finally, crosslinked microgels also exhibit a dense incompressible core, a feature that cannot be captured by a Hertzian. In a past study, we developed the so-called square-shoulder Hertzian V_{SSH} to address the last point (Schmidt et al. 2023). This model adds a square-shoulder term to account for the incompressible limit at a distance d_{core} (Sandoval-Puentes et al. 2022) and a transitional linear regime which models the core size of the microgel in the uncompressed state d_{out}. Finally, a more descriptive level is achieved with the total square-shoulder multi-Hertzian potential, $V_{SSMH}(r)$, written in Eq. 3. All parameters describing the square-shoulder are taken from Ref. (Sandoval-Puentes et al. 2022; Schmidt et al. 2023), with $A_\gamma = \gamma\left(\frac{\gamma}{\gamma-1}\right)^{\gamma-1}$, $B_\gamma = \frac{\gamma}{\gamma-1}$, $K = 10^4$, $\gamma = 50$, $\alpha = 0.354$, $T^* = 1.474$, $\epsilon_{ss} = k_B T$ (being k_B the Boltzmann constant and T the temperature) and $r_0 = \left(d_{out} - \sqrt{\frac{-\log\alpha}{K}}\right) d$. The constant or linear terms $V_H(r_0)$ and $F_H(r_0 - r)$ are added to keep the function continuous to use it in the context of molecular dynamics simulation. A comparison of these four different potential interactions is shown in Fig. 1(a).

We start with a validation of the potential for 5 mol% crosslinked microgels against experiments. Next, we vary the potential parameters in order to assess their individual effect on the rheological properties of the system. To this aim, for simplicity, we assume that the region between soft inner core and compressible limit is a constant $d_{out} - d_{core} = 0.2d$, which is approximately what we find for 5 mol% crosslinked microgels. In this way, we obtain only three free parameters that we can vary: Y, Y_{dens} and d_{core}. Their respective influence on the form of the potential is demonstrated in Fig. 1(b)-to-(d).

$$V_{SSMH}(r) = \begin{cases} \frac{A_\gamma}{T^*}\left[\left(\frac{d}{r}\right)^\gamma - \left(\frac{d}{r}\right)^{\gamma-1}\right] + \frac{1}{T^*} + \epsilon_{ss} + V_{MH}(r_0) + F_{MH}(r_0 - r) & \text{for } r < d_{core} B_\gamma \\ \epsilon_{ss} + V_{MH}(r_0) + F_{MH}(r_0 - r) & \text{for } d_{core} B_\gamma \le r < r_0 \\ \epsilon_{ss} \exp\left[-K(r - r_0)^2\right] + V_{MH}(r) & \text{for } r_0 \le r < d \\ 0 & \text{for } d \le r \end{cases} \tag{3}$$

We perform molecular dynamics simulations of systems with $N = 10000$ particles of mass m. The analysis focuses on the influence of interparticle interactions as a function of the generalized area fraction $\zeta_{2D} = \frac{\pi}{4A}\sum_i^N d_i^2$, where A denotes the area of the simulation box. We consider polydisperse

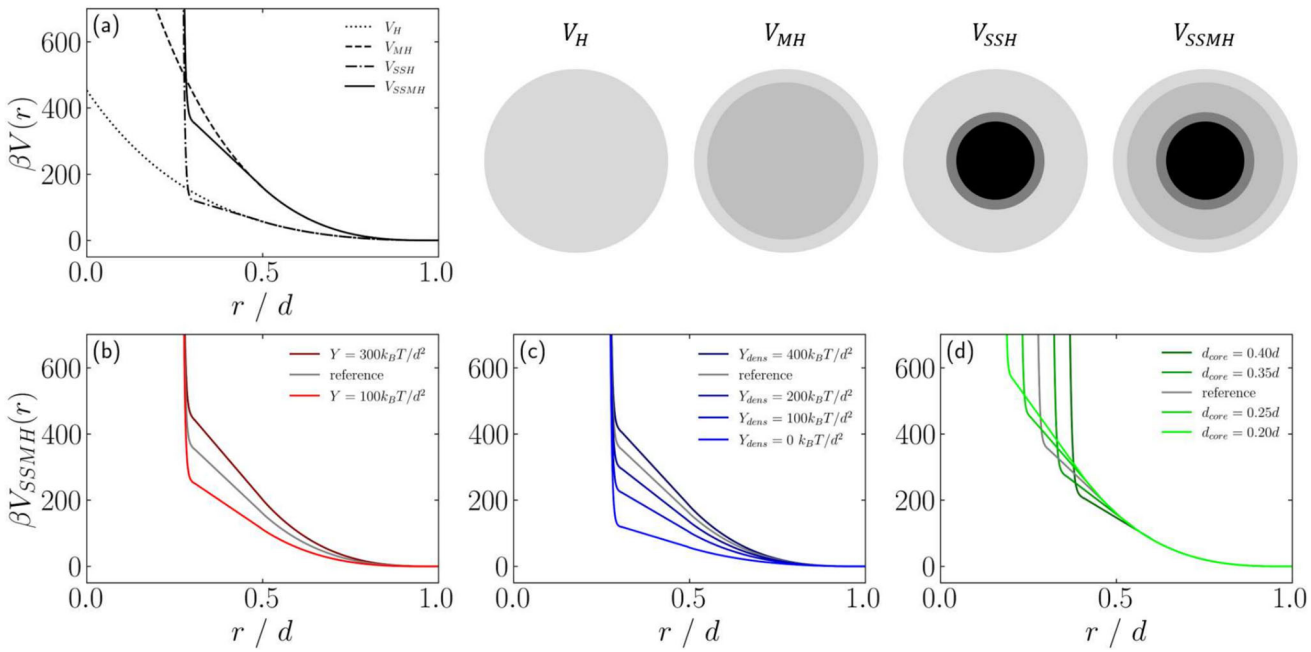

Fig. 1 (a) Evolution of the interaction potential as a function of the level of detail in the coarse-graining model and corresponding sketches. The square-shoulder multi-Hertzian potential, $\beta V_{SSMH}(r)$, described by Eq. 3, is plotted for $Y = 300k_BT/d^2$, $Y_{dens} = 300k_BT/d^2$ and $d_{core} = 0.3d$, and used as reference for the subsequent panels. Thus, Y (b), Y_{dens} (c) and d_{core} (d) are varied individually

systems to establish a comparison with the experimental case by choosing 50 discrete particle sizes with abundance according to a Gaussian distribution with standard deviation $\sigma = 10$ mol%. Thus, for two particles i and j interacting, the effective diameter is $d = (d_i + d_j)/2$, which directly influences Hertzian interaction strength and the size of the various core regions. Considering ϵ as the energy scale, the time is $\tau = \sqrt{\frac{md^2}{\epsilon}}$. Simulations are performed in the canonical ensemble at temperature $T = \epsilon/k_B$ controlled by a Langevin thermostat with damping parameter $\xi = 100\, m/\tau$.

The rheological behavior is studied by performing non-equilibrium simulations. In particular, we impose two different deformations: on the one hand, we apply linear deformations by imposing a shear rate $\dot{\gamma}$; on the other hand, we impose oscillatory deformations in the form of a sine wave, i.e. $\gamma\,(t) = \gamma_0 \sin(\omega t)$, where γ_0 is the strain amplitude, and ω corresponds to the angular frequency. In both cases, the deformations are applied upon the xy-plan, with x being the direction of the flow and a velocity gradient along y. During the deformations, we compute the shear stress from a micro-state by using the Irving-Kirkwood expression,

$$\sigma_{xy} = \frac{1}{A}\left(\sum_{i=1}^{N}\left[m_i v_{i,x} v_{i,y} + \sum_{j>i}^{N} r_{ij,x} f_{ij,y}\right]\right), \tag{4}$$

where v_x and f_y describe the respective component of the velocity and the force. In the steady shear deformations, the stress first overcomes a maximum with increasing strain, the yielding, until reaching a constant plateau stress during viscous flow. This plateau stress scales with the shear rate to result in a simple Herschel-Bulkey scaling law

$$\sigma_{plateau}\,(\dot{\gamma}) = \sigma_y + k\dot{\gamma}^n \tag{5}$$

where σ_y is the yield stress, while k and n are fitting parameters. For oscillatory deformations, we set $\gamma_0 = 3$ mol%, corresponding to the linear regime (Ketz et al. 1988). Then, we perform the simulation equivalent of a frequency sweep with angular frequencies in the range $\omega \in \left[10^{-1} - 10^{1}\right]\tau^{-1}$. A time dependent stress signal is obtained as the result, which can be used to compute storage, G', and loss modulus, G'' (Colombo and Del Gado 2014).

$$G'(\omega) = Re\left(\frac{\bar{\sigma}}{\bar{\gamma}}\right) \tag{6}$$

$$G''(\omega) = Im\left(\frac{\bar{\sigma}}{\bar{\gamma}}\right) \tag{7}$$

Here, $\bar{\sigma}$ and $\bar{\gamma}$ denote the Fourier transformations of the stress and shear strain signals.

Both equilibrium and non-equilibrium simulations are carried out using LAMMPS (Thompson et al. 2022), with a simulation time step $\delta t = 0.0005\tau$.

Results

Validation for 5 mol% crosslinked microgels

In the first step, the model potential is applied to an experimental system consisting of $c = 5$ mol% microgels that have a radius of 675 nm when spread at an interface. Radial distribution functions were measured using dry-state atomic force microscopy, and monolayer stiffness was characterized using interfacial shear rheology at the oil-water interface. Details of the experimental setup and data can be found in Ref. (Schmidt et al. 2023). The behavior of the monolayer is usually described in terms of five different regimes depending on the generalized area fractions, as described in detail elsewhere (Rey et al. 2016). From the measured radial distribution functions, the nearest neighbor distance d_{NN} can be extracted (see circles in Fig. 2). These data show that the coronas of microgels can be continuously compressed as ζ_{2D} increases, reaching distances significantly shorter than the size of the uncompressed particle. This happens until $\zeta_{2D} \simeq 2.2$, above which two distinct length scales emerge in the radial distribution function: at $d_{NN} \approx 375$ nm, the microgel coronas are entirely compressed, while $d_{NN} \approx 215$ nm represents the smallest measured distance between two microgels. This behavior has been successfully modeled in simulations using a square-shoulder Hertzian (SSH) (see squares in Fig. 2). In this model, the Hertzian component accounts for the deformation of the corona, while the square-shoulder term models the contact between cores. Since this is a hard boundary, it imposes that the corresponding distance denotes an incompressible core. Based on the experimental values, $d_{core} \sim 0.548d$ is the relative core size of the uncompressed microgel and $d_{out} \sim 0.318d$ represents the minimum distance between two microgels. The only remaining free parameter, which is the Young modulus controlling the strength of the Hertzian, was set in Ref. (Schmidt et al. 2023) to the value which best describes the behavior of the radial distribution function, i.e. $Y = 170k_BT/d^2$. Using this approach, the static properties of the monolayer are well captured at all generalized area fractions. We now consider, rather than a simple Hertzian, a multi-Hertzian potential plus a square shoulder (SSMH), with the additional parameter $Y_{dens} = 270k_BT/d^2$, accounting for the increase in monolayer stiffness when it is compressed. Also in this case, the characteristic nearest neighbor distances remain unaffected and still closely match experimental observations (see triangles in Fig. 2).

Nevertheless, the SSMH potential shows a significant advantage when modeling the behavior of a monolayer under shear. Indeed, now the system does not melt again upon increasing generalized area fraction in contrast to the SSH model and more similar to the experimental behavior. This is observed from linear continuous flow, from which the shear stress as a function of shear rate is obtained. The resulting flow curves are fitted using the Herschel-Bulkley scaling law and, by extrapolating to zero shear rate, the numerical yield stress σ_y is extracted. This is reported in Fig. 3 for SSH model (squares), for SSMH potential (circles) and from experimental flow curves (details in Ref. Schmidt et al. 2023). Qualitatively, all measured yield stresses have a similar non-monotonic dependence on ζ_{2D}. After an initial increase of the monolayer stiffness, marking a transition from the liquid to solid state, σ_y decreases and finally increases again. However, the V_{SSH} model predicts an intermediate re-entrant liquid phase, characterized by a sudden drop of the yield stress back to zero, where no external shear has to be applied for the system to flow. This particular behavior is not observed experimentally, where the decrease in monolayer stiffness is

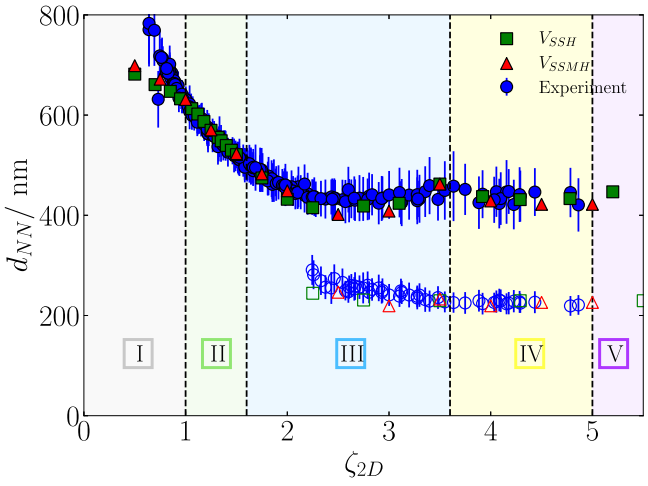

Fig. 2 Comparison of nearest neighbor distances d_{NN} extracted from experiment (circles), square-shoulder Hertzian (squares) and square-shoulder multi-Hertzian (triangles). Full symbols denote the regular phase while, empty figures describe the core-core contacts

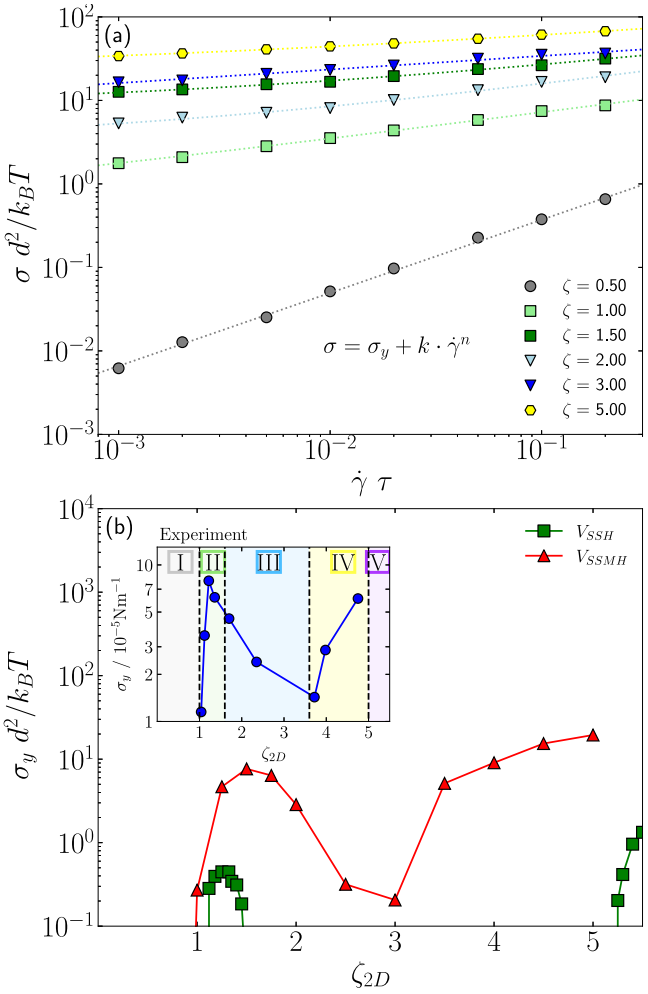

Fig. 3 Comparison of normalized yield-stress $\sigma_y d^2/k_BT$ extracted from experiment (circles in the inset), simulations using the square-shoulder Hertzian model (squares) or the square-shoulder multi-Hertzian model (triangles). Importantly, for the Hertzian model, the yield stress is zero in the regions where it is not shown, including state points for $1.5 \lesssim \zeta_{2D} \lesssim 5.0$

insufficient to melt the system, so that it remains a glassy solid for $\zeta_{2D} \geq 1.0$. This discrepancy can be attributed to several factors in the experimental system that are not captured by the simplicity of the V_{SSH} model. First, many-body interactions are neglected within a pair-potential approach. However, in a dense monolayer, the microgels are compressed by multiple neighbors, leading to a steeper increase in the individual particle stiffness than what is predicted by pairwise interactions alone. Second, the polymeric nature of microgels is not explicitly modeled at the micro-scale. Polymer chains in the outer corona may interpenetrate or interlock, increasing friction and enhancing stiffness in the system. Lastly, while the interface is effectively two-dimensional, it still possesses a finite thickness, which increases upon compression (Bochenek et al. 2022). Although the SSMH model also does not explicitly incorporate these effects, the additional Hertzian terms are able to effectively mimic their impact within the limitations of a pair potential based model. Thus, the use of the SSMH increases the interaction strength at intermediate particle-particle distances, and thus the overall stiffness of the system at higher deformation, which becomes relevant for high generalized area fractions. The parameters for this additional term ($Y_{dens} = 270\ k_BT/d^2$ & $d_{dens} = 0.9\ d$) are chosen empirically to ensure that the system maintains a yield stress above zero, correctly modeling a solid, but still preserving the behavior of the nearest-neighbour distance of the radial distribution function, as described above.

These results show that the SSMH, despite its simplicity, is able to qualitatively capture the experimental behavior of the microgel monolayers. While we have shown a comparison with $c = 5$ mol% microgels, our recent work (Ruiz-Franco et al. 2024) has shown a similar behavior for very soft ULC microgel. We can therefore adapt the SSMH as a generic simple model to describe the interfacial rheology of microgels monolayers and study their rheological properties in more detail upon varying the potential parameters in the next section.

Exploring the parameter space

After demonstrating that the proposed potential captures many of the static and dynamic properties of dense microgel monolayers, we now aim to predict how these properties change with variations of the characteristics of an individual microgel. Specifically, we focus on three factors: the stiffness of the corona of individual particles Y, the additional stiffness introduced by monolayer compression Y_{dens} and the size of the dense core d_{core}. The static properties are quantified once more using the radial distribution function, particularly its first peak, which corresponds to the nearest neighbor distance d_{NN}. The influence of the Young modulus on d_{NN} and on the peak height NN_{height} are shown in Fig. 4(a) and (d). Interestingly, both the nearest neighbor distance and the height of the peak are largely unaffected by changes in the Hertzian stiffness of the corona. Across all investigated values of the Young modulus, d_{NN} decreases continuously until core-core interactions become significant within the range $2.5 < \zeta_{2D} < 3.0$, as indicated by $d_{NN} < d_{out}$. At this point, an additional peak at distance d_{core} can be observed in the radial distribution function, characteristic for the core-core contacts (empty symbols). The similar trend of these graphs suggests that the Young modulus of the corona has only limited influence on the structure in equilibrium. In the regime dominated by corona-corona interactions ($\zeta_{2D} \leq 2.5$), stiffer coronas exhibit slightly stronger ordering, as indicated by the larger values of the peak height. Indeed, starting from the liquid state, the peak height increases up to $\zeta_{2D} \simeq 1.5$, after which it decreases. For $\zeta_{2D} \geq 3.0$, where core-core interactions dominate and two characteristic separation distances

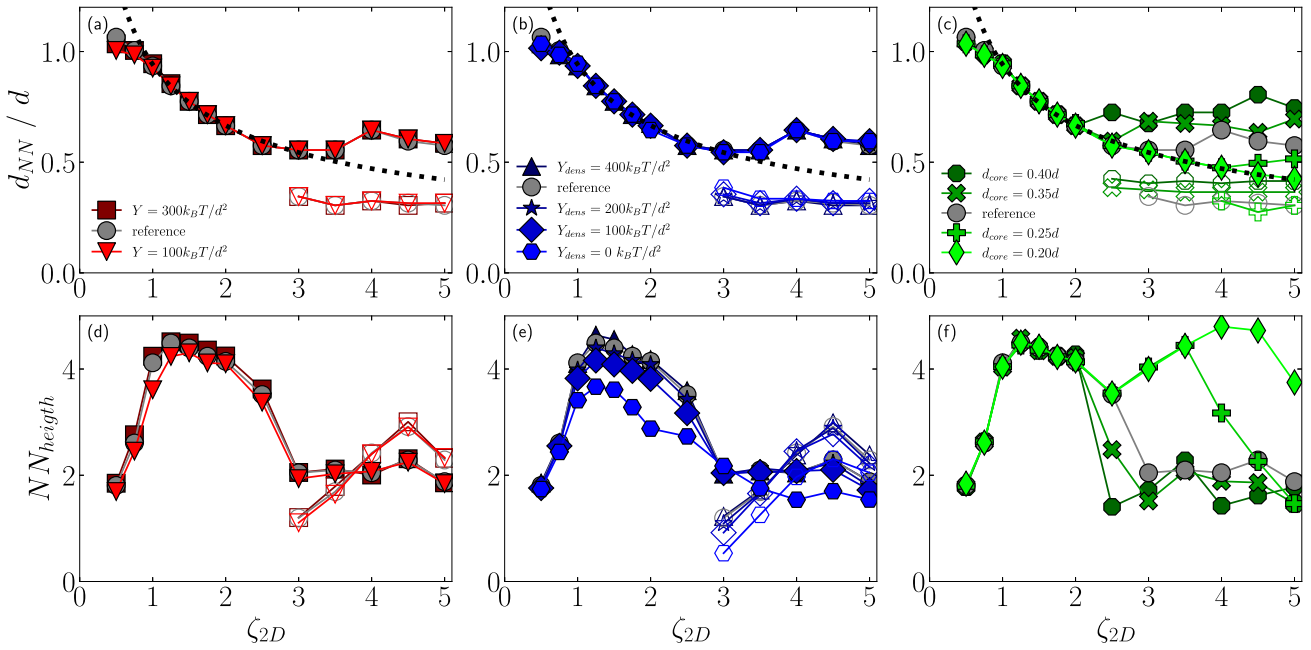

Fig. 4 Positions (a-c) and heights (d-f) of the nearest neighbor peaks, extracted from radial distribution functions. The regular phase is shown with full symbols and core-core contacts are depicted using empty symbols. Dotted lines in (a-c) represent $d_{NN} \propto \zeta_{2D}^{-1/2}$ scaling, which is expected for a regular Hertzian. The reference system (circles) is characterized by $Y = 200k_BT/d^2$, $Y_{dens} = 300k_BT/d^2$, $d_{core} = 0.3$ and $d_{out} = 0.4$. In (a & d), the Young's modulus is varied as a measure of corona stiffness, in (b & e) the monolayer stiffness is varied using the Y_{dens} parameter and in (c & f) the size of the core is varied at constant shoulder width $d_{out} - d_{core} = 0.2$

emerge in the radial distribution function, the absolute peak height diminishes (see Fig. S1) and stabilizes at a constant value. Instead, the number of core-core contacts increases, as can be seen by the increase in their peak height (empty symbols). Notably, this transition to core-core interactions is independent of the softness of the corona, resulting in identical peak heights for potentials with different Young moduli of the corona, as shown in Fig. 4(d).

Next, we examine the influence of Y_{dens}, representing the additional stiffness of the monolayer due to compression, in Fig. 4(b) and (e). The nearest-neighbor distance remains constant across the investigated Y_{dens} values, even when Y_{dens} is set to zero (hexagon symbols), effectively recovering the square-shoulder Hertzian model with a pronounced liquid regime. However, for $1.0 \leq \zeta_{2D} \leq 2.5$, higher values of Y_{dens} result in an increase of the heights of the peak. In this regime, the corona is already compressed, leading to increased stiffness, while core-core interactions have not yet begun.

The size of the dense microgel core (d_{core}) has the most significant impact on the monolayer's static arrangement, as illustrated in Fig. 4(c) and (f). Here, we compare potentials with different d_{core} parameter and a constant width of the shoulder $d_{out} - d_{core} = 0.2$ d. For microgels with small cores ($d_{core} = 0.2$ d and $d_{out} = 0.4$ d), represented by diamonds, the nearest-neighbor distance follows the typical Hertzian trend of an inverse square law, $\zeta_{2D}^{-1/2}$, as the cores never come into contact within the investigated range of generalized area fractions. For larger cores, the nearest-neighbor distance deviates from the Hertzian behavior once $d_{NN} < d_{out}$, at which point a secondary phase with a characteristic separation distance of d_{core} emerges (empty symbols). The square-shoulder term enables fine-tuning of the characteristic length scales within the monolayer. This structuring is also evident in the nearest-neighbor peak heights. While the cores remain non-interacting, the peaks follow a similar trend and deviations occur once the secondary core-core phase appears.

In order to determine how the potential parameters influence the rheological properties, we next examine the behavior of the storage modulus of the dense monolayer (see Fig. 5). Similarly to the yield stress, the storage modulus exhibits a non-monotonic behavior with increasing generalized area fraction: it increases up to $\zeta_{2D} = 1.5$, then decreases to $\zeta_{2D} = 2.5$ and finally increases again. As a consequence the monolayer shows some curious behavior, where it stores the same amount of energy at vastly different degrees of compression, we recently named the values of ζ_{2D} where this happens isoelastic points (Ruiz-Franco et al. 2024). When changing the Young modulus of the corona, a straightforward trend can be observed in Fig. 5(a), where an increase in corona stiffness also increases the storage modulus at all generalized area fractions, as the corona is the first part of the microgel to be compressed.

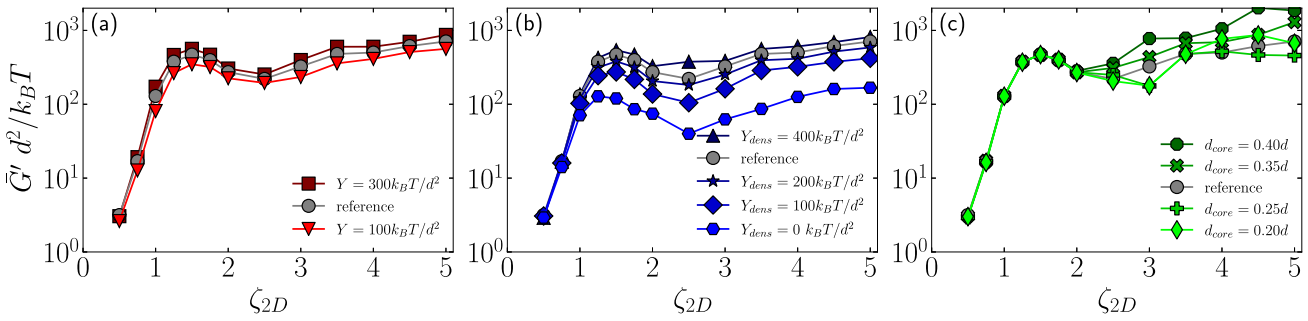

Fig. 5 Storage modulus for extracted from oscillatory shear computations with a strain amplitude of $\gamma_0 = 0.03$ and an angular frequency of $\omega = 0.2\tau^{-1}$. The reference system (circles) is characterized by $Y = 200k_BT/d^2, Y_{dens} = 300k_BT/d^2, d_{core} = 0.3\,\mathrm{d}$ and $d_{out} = 0.4\,\mathrm{d}$. In (a), the Young's modulus is varied as a measure of corona stiffness, in (b) the monolayer stiffness is varied using the Y_{dens} parameter and in (c) the size of the core is varied at constant shoulder width $d_{out} - d_{core} = 0.2\,\mathrm{d}$

Of more interest is the influence of Y_{dens}, depicted in Fig. 5(b) because this parameter does not have a clear relation to the architecture of an individual microgel. While the storage moduli are similar at $\zeta_{2D} \leq 0.75$, once the systems are more compressed, G' is larger for a higher value of Y_{dens}. This goes with expectations, since the intended purpose of the multi-Hertzian modification to the potential is to increase the stiffness of the monolayer once it is compressed. This trend persists even in the core-core interaction regime, since the energy needed to compress the monolayer is still stored. It is worth noting that the storage modulus alone cannot be used as a definitive criterion to identify the phase behavior. For instance, at generalized area fractions of 1.5 and 4, the storage moduli are similar for $Y_{dens} = 0$ (hexagon symbols), despite the system being solid for the former and liquid for the latter.

The influence of the size of the dense core is finally illustrated in Fig. 5(c). From the nearest neighbor distances, we know at which generalized area fraction the secondary phase, characterized by core-core contacts, forms. Once it is present, the storage modulus increases strongly with generalized area fraction, as can be clearly seen from the behavior of G' for the largest investigated $d_{core} = 0.4$ d (octagon symbols). Interestingly, even for Hertzian-style potentials without an incompressible core, a moderate increase in the storage modulus is still observed. This is evident here for $d_{core} = 0.2$ d (diamonds) where no core-core interactions are observed within the investigated range of generalized area fractions, yet the storage modulus still increases.

Variation of crosslinking

After having examined the impact of individual parameters of the model on the phase behavior and rheological properties of the monolayer, we now try to construct representative potentials for microgels with different crosslinker fractions c. We base our choice of parameters on the two available experimental measurements for 5 mol% crosslinked microgels, which were already used to validate the potential in Section "Validation for 5 mol% crosslinked microgels", and for ultra low crosslinked (ULC) microgels. It should be kept in mind that these two kinds of microgel adsorb differently to the interface: crosslinked microgels have a typical "fried egg"-structure with a core-corona architecture (Scotti et al. 2019; Camerin et al. 2019), while ULC microgels adsorb as a more flat and homogeneous "pancake" (Scotti et al. 2019; Bochenek et al. 2022). While for ULC microgels there is no additional crosslinking molecule in the synthesis, some self-crosslinks between NIPAM chains still occurs due to atom abstraction mechanism (Brugnoni et al. 2019). Therefore, we use the ULC microgels as the limiting case of a microgel with minimal crosslinking that can be obtained *via* precipitation polymerization ($c \lesssim 0.3$ mol% Lopez and Richtering 2017; Hazra et al. 2023). In general, one expects that the Young modulus of gels linearly scales with the number of crosslinks (De Gennes 1979). If we assume a similar scaling for microgels adsorbed at an interface, it is possible to simply extrapolate the Young modulus of the microgel corona between the two considered cases. For the core, two parameters have to be considered: d_{out} describing the size of the core in the uncompressed state and d_{core} representing the incompressible limit.

For crosslinked microgels in bulk it has been shown that their density profiles can be rescaled to a master curve by accounting for size and core density (Hazra et al. 2023). This would imply that they have similar relative core sizes in bulk. Whether this property remains once adsorbed to an interface has not yet been measured experimentally, however simulation results suggest that the relative core sizes should be very similar in 2D as well Camerin et al. (2019). Based on these considerations, we keep d_{out} fixed for microgels of different c. In contrast, d_{core} depends on the microgel once it has been compressed to its limit. Since more crosslinked microgels have higher density in the dilute state, they have to be

Table 1 Square shoulder multi-Hertzian parameters for microgels of different crosslink fraction. ULC microgels ("0 mol%") and 5 mol% crosslinked microgels are fitted to experiment, from which the remaining parameters were derived as described in the text

c (mol%)	Y/k_BTd^{-2}	Y_{dens}/k_BTd^{-2}	d_{core}/d	d_{out}/d
0	100	270	0.00	0.00
1	114	270	0.14	0.55
5	170	270	0.32	0.55
10	240	270	0.45	0.55

compressed less until they reach the incompressible limit and d_{core} is bigger. Hence, starting from a linear scaling of microgel density with c, we get $\sqrt{c} \propto d_{core}$. Finally, Y_{dens} has to be adjusted empirically so that it prevents the reentrance to the liquid phase at all generalized area fractions, which results for all chosen potentials in approximately the same value of $Y_{dens} \approx 270 k_BTd^{-2}$. Whether this parameter changes for different microgel crosslinking is currently unclear and for this study, it will be set constant to this minimum value, necessary to prevent a re-entrant fluid. A summary of the SSMH potential parameters as a function of c is reported in Table 1.

Using the determined parameters, we calculate the nearest neighbor distance, storage modulus and yield stress, following the procedures described previously. The results are summarized in Fig. 6. We start by discussing d_{NN} as a function of c, reported in Fig. 6(a). We see that after an initial decrease, compatible with isotropic shrinking as $\sim \zeta_{2D}^{-1/2}$, for $\zeta_{2D} \gtrsim 2.0$, the behaviors become different according to the value of c. For large crosslink fractions the core-core distances (empty symbols) are larger, since they reach their incompressible limit earlier. Indeed, for $c = 10$ mol% (square symbols), the incompressible core is similar in size to the size predicted by isotropic shrinking. At $\zeta_{2D} = 5.0$, the microgels would need to be smaller than d_{core} and the simulation does not predict meaningful results. The experimental equivalent would be the destruction of the monolayer. Interestingly, for $c = 1$ mol% (circles) there is a non-monotonic behavior of d_{NN} for $\zeta_{2D} \sim 3.5$ due to the competition between the two length scales, since in this case the square shoulder width is significantly large.

Turning to examine the behavior of the storage modulus in Fig. 6(b), we find a slight increase of G' with c, in agreement with experimental measurements (Rey et al. 2023;

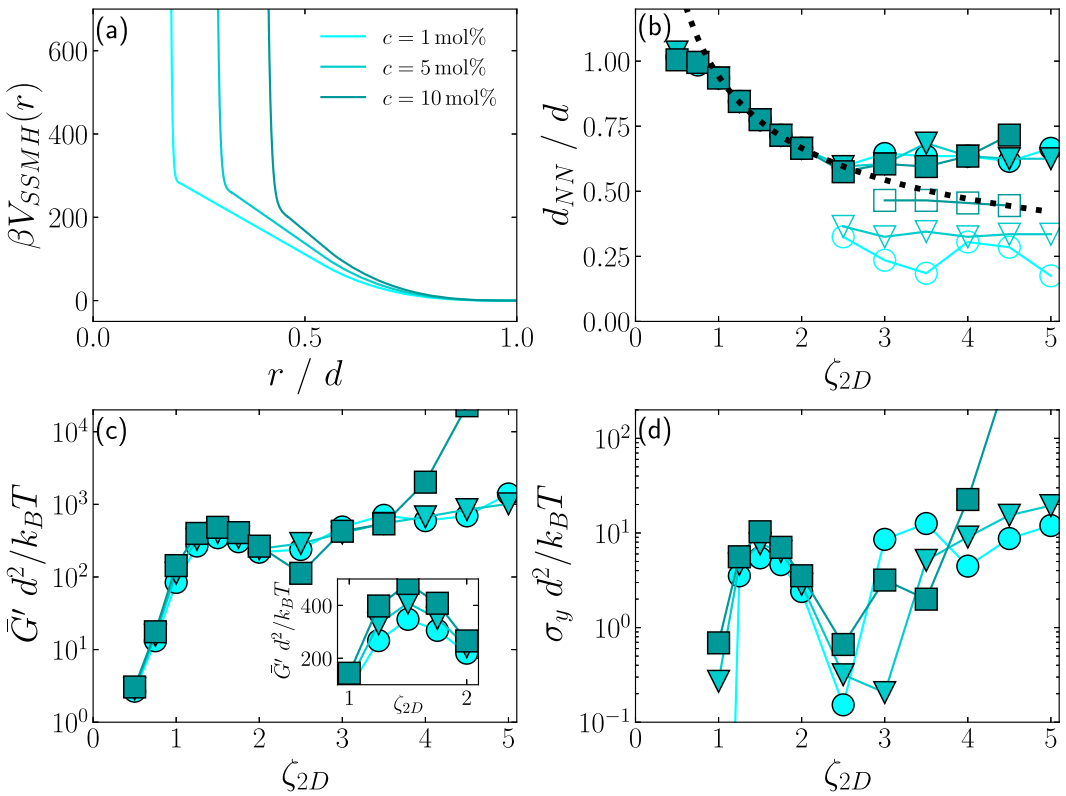

Fig. 6 Monolayer properties as predicted for a model set of parameters, which represent different microgel crosslinking fractions (see Table 1): $c = 10$ mol% (squares), $c = 5$ mol% (triangles) and $c = 1$ mol% (circles). The corresponding effective SSMH potentials are plotted in (a). In (b), the nearest neighbor distance extracted from the radial distribution function is depicted. Filled symbols are normal contacts and the dotted line reflects a $d_{NN} \propto \zeta_{2D}^{-1/2}$ scaling; hollow symbols denote the onset of core-core contacts. In (c) and (d) the storage modulus and the yield stress are plotted, respectively

Schmidt et al. 2023; Ruiz-Franco et al. 2024) with the non-monotonicity occurring roughly always in the same range of generalized area fractions. Interestingly, the non-monotonic behavior seems to be more pronounced for $c = 10$ mol%, a prediction that awaits for experimental confirmation in the future. Finally, as expected, for very larger ζ_{2D}, G' increases again with a growth that is much more pronounced for stiffer microgels, which reach the incompressible limit earlier and have more core-core contacts.

Next, we report the yield stress in Fig. 6(c), which displays a similar behavior to G' and confirms that the monolayers remain solid at all values of $\zeta_{2D} > 1.0$ as expected from experiments. Here, the growth of the modulus with c is more evident. Then, the non-monotonicity occurs for all studied crosslinker concentrations, in analogy with experiments. A further increase of ζ_{2D} yields a second bump in the curves, perhaps due to the multi-Hertzian character of the potential or core-core contacts. This was not reported in experiments, but perhaps several data points in ζ_{2D} should be probed in order to visualize such a subtle effect. Overall, the results behave within the expectations, awaiting for further experimental studies to confirm the validity and the limitations of the SSMH model.

Conclusion

In this work we examined the rheological properties of microgel monolayers, when confined at a liquid-liquid interface, e.g. oil-water (Camerin et al. 2019) or air-water (Bochenek et al. 2022). We first established the square-shoulder-multi-Hertzian (SSMH) model as the simplest model able to capture the main features observed in experiments as a function of generalized area fraction. In particular, the monolayers are found to undergo a liquid-to-solid transition for $\zeta_{2D} \lesssim 1.0$, then they remain solid for $\zeta_{2D} > 1$ but with elastic properties which show a non-monotonic dependence on ζ_{2D}. The use of a multi-Hertzian term is crucial to maintain the solid-like character of the monolayer, preventing the peculiar reentrance to a liquid state predicted by the simple Hertzian model. Nonetheless, such reentrance manifests itself as a non-monotonic behavior of the yield stress or storage modulus as a function of ζ_{2D}, as already discussed in Ref. (Ruiz-Franco et al. 2024).

We then take advantage of computer simulations and explore the influence of the different parameters of our potential on the structural and rheological properties of the monolayer. We thus try to model monolayers of microgels with different values of the crosslinker concentration, not yet investigated experimentally. While we find that the non-monotonicity of the elastic moduli is preserved at all c, we also confirm that stiffer microgels give rise to overall stiffer monolayers, in agreement with expectations and with experimental results (Schmidt et al. 2023; Rey et al. 2023; Ruiz-Franco et al. 2024) . Given the multiple approximations made in the development of the SSMH model and of the many involved parameters, it would be very interesting in the future to carry out additional measurements to compare with the present simulations. Furthermore, interfacial rheology measurements should be extended to microgels of different architectures, e.g. hollow ones, or with different charge content, in order to further tune the response of the monolayer as function of compression and to assess whether the collective rheological behavior is still linked to the single-particle one. This will be the subject of future work.

Supplementary Information The online version contains supplementary material available at https://doi.org/10.1007/s00397-025-01503-0.

Acknowledgements AS acknowledge financial support from the Knut and Alice Wallenberg Foundation (Wallenberg Academy Fellows). J.R.-F thanks the Department of Research and Universities of the Generalitat de Catalunya through Beatriu de Pinós program Grant (Contract No. 2022 BP 00156). The authors gratefully acknowledge financial support from the Deutsche Forschungsgemeinschaft (DFG) withing the SFB 985 "Functional microgels and microgel systems". The authors thank the RWTH Aachen University that granted the computation time under project rwth0946.

Data Availability All data needed to evaluate the conclusions in the paper are present in the paper and/or the Supplementary Materials. Additional data related to this paper may be requested from the authors.

References

Bachman H, Brown AC, Clarke KC, Dhada KS, Douglas A, Hansen CE, Herman E, Hyatt JS, Kodlekere P, Meng Z et al (2015) Ultrasoft, highly deformable microgels. Soft Matter 11(10):2018–2028

Bassu G, Houston JE, Lara-Peña MA, Kriegs H, Lettinga MP, Porcar L, Scotti A, Laurati M (2024) Link between permanent shear-banding and local concentration fluctuations in suspensions of compressible microgels. Phys Fluids 36(11)

Bergman MJ, Gnan N, Obiols-Rabasa M, Meijer J-M, Rovigatti L, Zaccarelli E, Schurtenberger P (2018) A new look at effective interactions between microgel particles. Nat Commun 9(1):5039

Berthier L, Moreno AJ, Szamel G (2010) Increasing the density melts ultrasoft colloidal glasses. Phys Rev E-Stat Nonlin Soft Matter Phys 82(6):060501

Bochenek S, Camerin F, Zaccarelli E, Maestro A, Schmidt MM, Richtering W, Scotti A (2022) In-situ study of the impact of temperature and architecture on the interfacial structure of microgels. Nat Commun 13(1):3744

Brugnoni M, Nickel AC, Kröger LC, Scotti A, Pich A, Leonhard K, Richtering W (2019) Synthesis and structure of deuterated ultra-low cross-linked poly (n-isopropylacrylamide) microgels. Polymer Chem 10(19):2397–2405

Camerin F, Fernández-Rodríguez MA, Rovigatti L, Antonopoulou M-N, Gnan N, Ninarello A, Isa L, Zaccarelli E (2019) Microgels adsorbed at liquid-liquid interfaces: a joint numerical and experimental study. ACS Nano 13(4):4548–4559

Camerin F, Gnan N, Ruiz-Franco J, Ninarello A, Rovigatti L, Zaccarelli E (2020) Microgels at interfaces behave as 2d elastic particles featuring reentrant dynamics. Phys Rev X 10(3):031012

Colombo J, Del Gado E (2014) Stress localization, stiffening, and yielding in a model colloidal gel. J Rheol 58(5):1089–1116

Conley GM, Aebischer P, Nöjd S, Schurtenberger P, Scheffold F (2017) Jamming and overpacking fuzzy microgels: deformation, interpenetration, and compression. Sci adv 3(10):1700969

Crassous JJ, Mihut AM, Månsson LK, Schurtenberger P (2015) Anisotropic responsive microgels with tuneable shape and interactions. Nanoscale 7(38):15971–15982

De Gennes P-G (1979) Scaling concepts in polymer physics. Cornell university press

Del Monte G, Zaccarelli E (2024) Numerical study of neutral and charged microgel suspensions: from single-particle to collective behavior. Phys Rev X 14(4):041067

Gerelli Y, Camerin F, Bochenek S, Schmidt MM, Maestro A, Richtering W, Zaccarelli E, Scotti A (2024) Softness matters: effects of compression on the behavior of adsorbed microgels at interfaces. Soft Matter 20(17):3653–3665

Hazra N, Ninarello A, Scotti A, Houston JE, Mota-Santiago P, Zaccarelli E, Crassous JJ (2023) Structure of responsive microgels down to ultralow cross-linkings. Macromolecules 57(1):339–355

Höfken T, Gasser U, Schneider S, Petrunin AV, Scotti A (2024) Real and in silico microgels show comparable bulk moduli below and above the volume phase transition. Macromol Rapid Commun 2400043

Houston JE, Fruhner L, Cotte A, Rojo González J, Petrunin AV, Gasser U, Schweins R, Allgaier J, Richtering W, Fernandez-Nieves A et al (2022) Resolving the different bulk moduli within individual soft nanogels using small-angle neutron scattering. Sci Adv 8(26):6129

Huang S, Gawlitza K, Klitzing R, Steffen W, Auernhammer GK (2017) Structure and rheology of microgel monolayers at the water/oil interface. Macromolecules 50(9):3680–3689

Karg M, Wellert S, Pastoriza-Santos I, Lapp A, Liz-Marzán LM, Hellweg T (2008) Thermoresponsive core-shell microgels with silica nanoparticle cores: size, structure, and volume phase transition of the polymer shell. Phys Chem Chem Phys 10(44):6708–6716

Karg M, Pich A, Hellweg T, Hoare T, Lyon LA, Crassous J, Suzuki D, Gumerov RA, Schneider S, Potemkin II et al (2019) Nanogels and microgels: from model colloids to applications, recent developments, and future trends. Langmuir 35(19):6231–6255

Ketz R, Prud'homme R, Graessley W (1988) Rheology of concentrated microgel solutions. Rheol Acta 27:531–539

Lopez CG, Richtering W (2017) Does flory-rehner theory quantitatively describe the swelling of thermoresponsive microgels? Soft Matter 13(44):8271–8280

Lyon LA, Fernandez-Nieves A (2012) The polymer/colloid duality of microgel suspensions. Ann Rev Phys Chem 63(1):25–43

Lyon LA, Meng Z, Singh N, Sorrell CD, John AS (2009) Thermoresponsive microgel-based materials. Chem Soc Rev 38(4):865–874

Nayak S, Gan D, Serpe MJ, Lyon LA (2005) Hollow thermoresponsive microgels. Small 1(4):416–421

Pàmies JC, Cacciuto A, Frenkel D (2009) Phase diagram of hertzian spheres. J Chem Phys 131(4)

Philippe A-M, Truzzolillo D, Galvan-Myoshi J, Dieudonné-George P, Trappe V, Berthier L, Cipelletti L (2018) Glass transition of soft colloids. Phys Rev E 97(4):040601

Plamper FA, Richtering W (2017) Functional microgels and microgel systems. Accounts Chem Res 50(2):131–140

Purnomo EH, Ende D, Vanapalli SA, Mugele F (2008) Glass transition and aging in dense suspensions of thermosensitive microgel particles. Phys Rev Lett 101(23):238301

Rey M, Fernández-Rodríguez MÁ, Steinacher M, Scheidegger L, Geisel K, Richtering W, Squires TM, Isa L (2016) Isostructural solid-solid phase transition in monolayers of soft core-shell particles at fluid interfaces: structure and mechanics. Soft Matter 12(15):3545–3557

Rey M, Fernandez-Rodriguez MA, Karg M, Isa L, Vogel N (2020) Poly-n-isopropylacrylamide nanogels and microgels at fluid interfaces. Acc Chem Res 53(2):414–424

Rey M, Kolker J, Richards JA, Malhotra I, Glen TS, Li ND, Laidlaw FH, Renggli D, Vermant J, Schofield AB et al (2023) Interactions between interfaces dictate stimuli-responsive emulsion behaviour. Nat Commun 14(1):6723

Rovigatti L, Gnan N, Ninarello A, Zaccarelli E (2019) Connecting elasticity and effective interactions of neutral microgels: the validity of the hertzian model. Macromolecules 52(13):4895–4906

Ruiz-Franco J, Höfken T, Schmidt MM, Bochenek S, Zaccarelli E, Scotti A (2024) Very soft microgels at the interface behave and flow as hertzian-like spheres. arxiv:2501.09472

Sandoval-Puentes MA, Torres-Carbajal A, Zavala-Martínez AB, Castañeda-Priego R, Méndez-Alcaraz JM (2022) Soft representation of the square-well and square-shoulder potentials to be used in brownian and molecular dynamics simulations. J Phys Cond Matter 34(16):164001

Sbeih S, Mohanty PS, Morrow MR, Yethiraj A (2019) Structural parameters of soft pnipam microgel particles as a function of crosslink density. J Colloid Interface Sci 552:781–793

Schmidt MM, Ruiz-Franco J, Bochenek S, Camerin F, Zaccarelli E, Scotti A (2023) Interfacial fluid rheology of soft particles. Phys Rev Lett 131(25):258202

Schulte MF, Izak-Nau E, Braun S, Pich A, Richtering W, Göstl R (2022) Microgels react to force: mechanical properties, syntheses, and force-activated functions. Chem Soc Rev 51(8):2939–2956

Scotti A, Bochenek S, Brugnoni M, Fernandez-Rodriguez M-A, Schulte MF, Houston J, Gelissen AP, Potemkin II, Isa L, Richtering W (2019) Exploring the colloid-to-polymer transition for ultra-low crosslinked microgels from three to two dimensions. Nat Commun 10(1):1418

Scotti A, Brugnoni M, Lopez CG, Bochenek S, Crassous JJ, Richtering W (2020) Flow properties reveal the particle-to-polymer transition of ultra-low crosslinked microgels. Soft Matter 16(3):668–678

Scotti A, Schulte MF, Lopez CG, Crassous JJ, Bochenek S, Richtering W (2022) How softness matters in soft nanogels and nanogel assemblies. Chem Rev 122(13):11675–11700

Scotti A, Brugnoni M, Rudov A, Houston J, Potemkin I, Richtering W (2018) Hollow microgels squeezed in overcrowded environments. J Chem Phys 148(17)

Stieger M, Lindner P, Richtering W (2004) Structure formation in thermoresponsive microgel suspensions under shear flow. J Phys Cond Matter 16(38):3861

Stieger M, Pedersen JS, Lindner P, Richtering W (2004) Are thermoresponsive microgels model systems for concentrated colloidal suspensions? a rheology and small-angle neutron scattering study. Langmuir 20(17):7283–7292

Thompson AP, Aktulga HM, Berger R, Bolintineanu DS, Brown WM, Crozier PS, Veld PJ, Kohlmeyer A, Moore SG, Nguyen TD, Shan R, Stevens MJ, Tranchida J, Trott C, Plimpton SJ (2022) LAMMPS - a flexible simulation tool for particle-based materials modeling at the atomic, meso, and continuum scales. Comp Phys Comm 271:108171. https://doi.org/10.1016/j.cpc.2021.108171